CRITICAL REVIEW

Check for updates

Trapping and control of bubbles in various microfluidic applications

Yuan Gao, [iD] [a] Mengren Wu,[a] Yang Lin [iD] [b] and Jie Xu [iD] *[a]

As a simple, clean and effective tool, micro bubbles have enabled advances in various lab on a chip (LOC) applications recently. In bubble-based microfluidic applications, techniques for capturing and controlling the bubbles play an important role. Here we review active and passive techniques for bubble trapping and control in microfluidic applications. The active techniques are categorized based on various types of external forces from optical, electric, acoustic, mechanical and thermal fields. The passive approaches depend on surface tension, focusing on optimization of microgeometry and modification of surface properties. We discuss control techniques of size, location and stability of microbubbles and show how these bubbles are employed in various applications. To finalize, by highlighting the advantages of these approaches along with the current challenges, we discuss the future prospects of bubble trapping and control in microfluidic applications.

1. Introduction

Bubbles have continued to attract attention and appeared in artistic works and the scientific literature for centuries.[1] Recently, bubbles have been widely employed for many applications ranging from materials science,[2–4] environment,[5] food industry,[6,7] engineering,[8] medicine[9,10] to life science.[11] With the development of microfluidics in recent years, micro/nano-scale bubbles have been considered as an emerging tool and have become a field of growing

interest for addressing many challenges in various Lab-on-a-Chip (LOC) applications.[12] For example, under an acoustic field, bubbles were remotely excited to act as a pump,[13,14] filter,[15] mixer[16] or transporter[17] in the fluid. Moreover, bubbles were also innovatively used to manipulate different kinds of particles for functional applications without contact,[18] such as cell separation,[19] drug delivery,[20,21] and water treatment.[22] Here, a bubble is considered a volume of gas inside a liquid phase or a solid phase.[23] Normally, due to surface tension, a free-standing micro-scale bubble would keep a spherical shape. In some cases, when a bubble is attached to a solid wall or excited by external fields, such as an acoustic field, the shape of the bubble is affected due to contact or force field. In microfluidics, bubbles are usually

[a] Department of Mechanical and Industrial Engineering, University of Illinois at Chicago, Chicago, USA. E-mail: jiexu@uic.edu
[b] Department of Mechanical, Industrial and Systems Engineering, University of Rhode Island, Kingston, USA
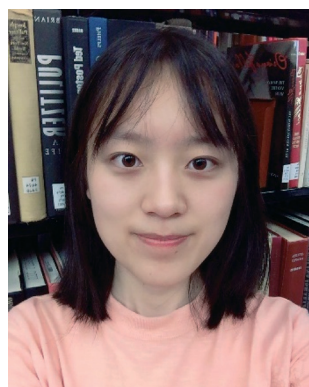
Yuan Gao is a Ph.D. student in mechanical engineering at the University of Illinois at Chicago (UIC). She received her B.S. from Chongqing University of Science and Technology in 2017 and M. S. from the University of Illinois at Chicago in 2018. She has been doing research at Prof. Xu's Microfluidics Laboratory at UIC. Her current research focuses on bubble-based microfluidics and its biomedical and chemical applications.

Yuan Gao
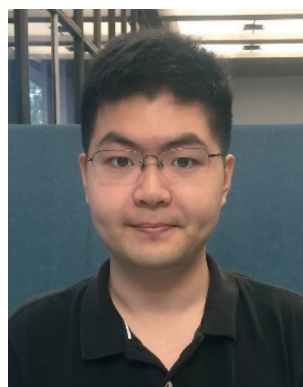
Mengren Wu obtained his B.S. in petroleum engineering from Chongqing University of Science and Technology, China in 2017 and M.S. in mechanical engineering from the University of Illinois at Chicago, United States in 2018. He is working as a Ph.D. student in Dr. Xu's Microfluidics Laboratory at the University of Illinois at Chicago and his research interests include electrokinetic phenomena in micro/nanofluidic

Mengren Wu

systems and acoustofluidics.

confined in a microchannel at low Reynolds numbers.[24] Bubbles could attain a suspended spherical shape if they are much smaller than the microchannel. If they are attached or confined by the microstructures of the microchannel, they will usually form a spherical cap. With the actuation of low and high acoustic energies, bubbles will respond to the actuation with linear and non-linear oscillations.[25–27] For instance, Marmottant *et al.* successfully used a linearly oscillated single bubble to generate microstreaming for single-cell lysis.[28] With high-intensity focused ultrasound (HIFU), nonlinear bubble oscillation was induced and employed for drug delivery and noninvasive therapy in tissues.[29] The strongest microstreaming occurs when the bubble oscillates at its resonant frequency. For a spherical microbubble, the resonant frequency can refer to Minnaeart's equation. In particular, the resonant frequency for an air–water bubble at atmospheric pressure and room temperature can be estimated from eqn (1). From the equation, the resonant frequency (kHz) of a bubble is inversely proportional to its radius (mm).[30]

$$f_0 \cong \frac{3.29}{R_0} \qquad (1)$$

As a low-cost and efficient tool, bubbles open a new door for tackling the challenges in microfluidics. Bubble-based applications have gained more and more attention since they are simple to fabricate and the bubbles are flexible to integrate with different microgeometries. In bubble-based microfluidic applications, the first and vital step is to effectively form and trap bubbles. Various methods have been explored for trapping bubbles in microfluidics. For example, external energy fields can be used to create and maintain bubbles, such as electro-chemical,[31,32] acoustic,[33] and opto-thermal methods.[34,35] Moreover, hydrophobic microchannels or microstructures were also employed to trap bubbles by modifying the surface wettability.[36] Due to surface tension, bubbles can be passively trapped in microcavities for microfluidic applications.[37] It is also important to fix bubbles in the desired location, with the desired size and lifetime in many bubble-based microfluidic applications, such as ultrasonic diagnosis, drug delivery, drag reduction, mass transport, micro-scaled sensing and actuation. However, there still exist challenges in controlling bubble size, location, and stability in many applications. Therefore, to obtain more robust and reliable performance of bubbles in microfluidics, it is of great significance to investigate techniques for controlling bubbles, including the stability, position and size of bubbles. The stability of bubbles has been studied in the past several years, which depends on the properties of bubbles, aqueous media, temperature, time, and pressure. The mechanisms of the instability include pressurization, pressure gradient, air diffusion, condensation, vibration, and wetting transition.[38–40] To address this issue, many researchers have investigated methods to enhance the lifetime of bubbles, such as using soluble surfactants or NaCl solutions, controlling saturation levels, designing structures to protect bubbles from dissolution, *etc.*[41–43] To precisely maintain bubbles at desired positions, researchers explored many approaches, such as using the properties of fluids and geometry of microchannels, creating artificial cavities, employing laser or electric energy to focus, *etc.* According to

Prof. Yang Lin received his Ph.D. degree in mechanical engineering from the University of Illinois at Chicago in 2019. He is currently an assistant professor of mechanical engineering at the University of Rhode Island. The overarching goal of his research is to develop fully integrated microfluidic analytical systems for environment monitoring, food safety analysis and biomedical applications. His research interests span from building low-

Yang Lin

cost microfluidic devices using off-the-shelf materials such as papers and plastic films to in vitro physiological studies using organ-on-a-chip platforms, and to on-chip flow and particle manipulation as well as deep learning-aided microfluidics.
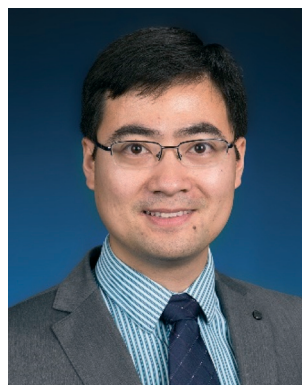
Prof. Jie Xu is an associate professor of mechanical engineering at the University of Illinois at Chicago. His research interest lies in microfluidics and lab-on-a-chip technology. He received his B.S. (2005) in thermal engineering from Tsinghua University, and both M.S. (2006) and Ph.D. (2010) degrees in mechanical engineering from Columbia University. Dr. Xu has published over 70 journal articles with a

Jie Xu

total of 2800+ citations, resulting in an H-index of 28. Dr. Xu is a recipient of a NASA Early Career Faculty Award and a DARPA Young Faculty Award. He is also an elected member of the Global Young Academy (GYA). He received multiple teaching and research awards from UIC, including a 2018 UIC Rising Star Researcher and Scholar of the Year Award. In 2019, Dr. Xu was named one of the 21 distinguished "Researchers to Know" by the Illinois Science and Technology Coalition (ISTC).

different bubble trapping methods, the size control strategy might be different. For example, the bubble size can be adjusted by controlling the flow rate of the gas and liquid supply, tuning the laser power or electric current, changing the frequency of the piezoelectric, altering the temperature and pressure applied to the channel or modifying the surface properties.

Bubbles can significantly impact experimental results by influencing flow behaviors. The use of bubbles benefits various applications due to the advantages of simplicity, controllability and biocompatibility. There exist several excellent reviews on generation and stabilization of microbubbles for ultrasonic imaging and medical therapy.[44–46] Bubble trapping and control techniques in microfluidics, however, have not been surveyed in the past.

In this review, we introduce and discuss bubble trapping and control techniques that have emerged and been employed in microfluidic applications during the last few years. These techniques can be classified into active and passive categories based on their dependence on external energy (Fig. 1). The active methods trap and control bubbles by external fields, such as acoustic, optical and electric fields. On the other hand, the passive trapping and control techniques depend on device geometries and surface properties. With this review, we hope to help researchers better perform bubble-based microfluidic experiments, serving as an inspiration of novel inventions in the future.

2. Active trapping and control techniques

With the aid of external energy inputs, active bubble trapping methods provide several advantages for various bubble-based microfluidic applications. For instance, active trapping methods offer flexible ways to control the position, size, and generation rate of bubbles. Moreover, with different trapping techniques, the properties of trapped bubbles can be varied, including air bubbles, vapor bubbles, nitrogen bubbles, oxygen bubbles and hydrogen bubbles, which could be applied according to the requirements. In this section, we classify the active bubble trapping and control methods based on the types of external fields: optical, electrical, thermal, magnetic, mechanical and acoustic (Table 1). We further discuss the different active trapping mechanisms, types of bubbles and their applications under external fields.

2.1 Optical control

Pulsed laser microbeams have been employed to trap bubbles in many microfluidic applications with the advantages of precise position control and size control. When an intense laser pulse is focused in a liquid medium, heated plasma is generated by the optical technique and then a bubble is formed at the focus point due to the rapid temperature increase. Once the bubble is created, it first expands to an almost perfect sphere and then collapses with subsequent rebounds. The
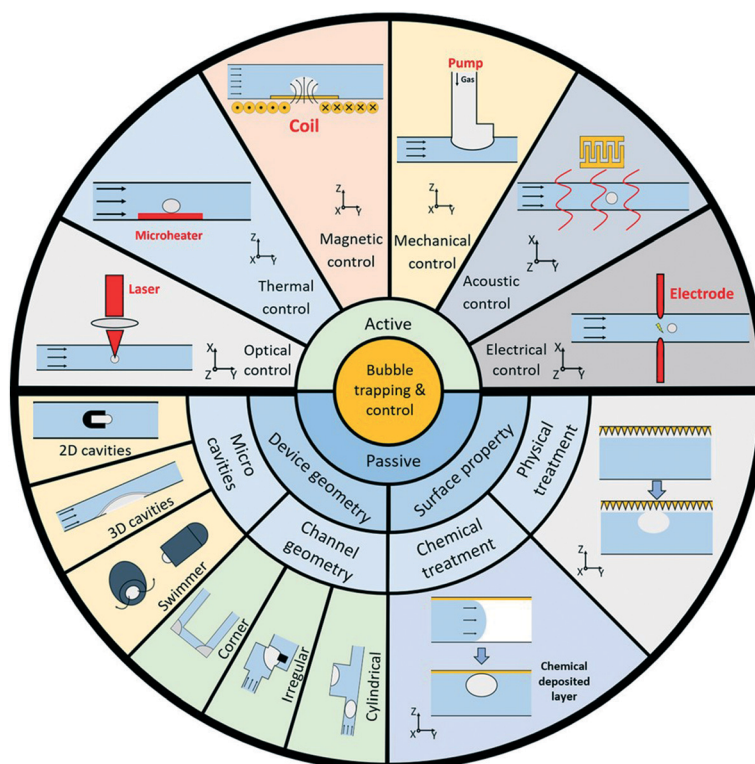

Fig. 1 Overview of common bubble trapping and control methods in microfluidics.

Lab on a Chip

Table 1 Comparison of different active bubble trapping and control techniques

Technique	Mechanism	Implementation and energy consumption	Type of bubble	Size of bubble (diameter)	Location of bubble	Performance	Application	Ref.
Optical	Optical force	Laser pulse and laser energy is tuned from 0 to 100 μJ	Vapor bubble	0–160 μm	Generate at arbitrary locations based on the laser spot locations	Bubble collapses and fully disappears within 20 μs	Cell sorting	49, 93
		Laser pulse and laser intensity is 508 kW cm^{-2}	Vapor bubble	0–9 μm		The bubble dissolves rapidly when the laser pulses cease	Cell poration	51
		Laser pulse combined with trapping structure and laser energy is 100 μJ	Vapor bubble	0–100 μm		The bubble collapses completely within 13.3 μs	Cell poration	50
	Photothermal conversion	Continuous-wave (CW) laser operation and laser power is 8–16 mW	Vapor bubble	0–60 μm		The bubble collapses quickly due to the flow	Fluid actuation	53
	Marangoni convection	Laser heating and laser power is 250 mW	Vapor bubble	200 μm, 570 μm and 700 μm (controlled by laser power)		Response time is one to tens of seconds and the bubble shrinks but does not collapse after the laser is turned off	Micropumps, microvalves	52, 94
Electrical	Electric force	Constant DC	Oxygen and hydrogen bubbles	5–20 μm	H$_2$ and O$_2$ bubbles are generated at the cathode side and the anode side, respectively	—	Microswimmers	75
	Electrochemical reaction	Electrolyzer control system and current densities are 20 mA cm^{-2} and 100 mA cm^{-2}	Oxygen and hydrogen bubbles	O$_2$ bubble: 40–80 μm; H$_2$ bubble: 30–70 μm (controlled by the current intensity and the flow rate)		The bubble gradually grows and eventually detaches from the surface of the electrode	Study of the bubble evolution mechanism	77
	Electrical force	Glass electrode and stiction force of the air–liquid interface and applied power is 15 W	Plasma bubble	—	Create on one side of the glass electrode	—	Gene transfer	95
	Electrochemical reaction	AC power supply and current is 20 μA	Air-buffer bubble	~75 μm	—	Bubble formation rate is influenced by applied current	Liquid interfacial tension measurement	96
Thermal	Evaporation	Heating and applied power is 3.4 W	Vapor bubble	0–350 μm	Generates on the micro line heater	The bubble grows to maximum in 30 ms and collapses in 0.6 s when voltage application to the heater ceases	Micropump	62
	Evaporation	High power heating and heat flux is 20.3 MW m^{-2}	Vapor bubble	Satellite bubble size: ~9 μm to 23 μm; primary bubble size: ~0–200 μm	Creates on the heater surface	The primary bubble shrinks to a minimum in tens of microseconds when the power is off and is removed from the heater under acoustic actuation	Study of thermal bubble dynamics	60
Magnetic	Electromagnetic force	Magnetic induction heating and applied power is 3 W	Vapor bubble	0–1 mm	Creates at the heating plate	The bubble shrinks in the 1 s condensation period and cannot disappear	Micropump	97

Table 1 (continued)

Technique	Mechanism	Implementation and energy consumption	Type of bubble	Size of bubble (diameter)	Location of bubble	Performance	Application	Ref.
Mechanical	Vacuum pressure	Vacuum and vacuum pressures are from −100 to −20 kPa	Oil–water bubble	1–7 μm	Suspend in the fluid	The bubble remains stable when the vacuum pressure is −60 and −70 kPa for at least 25 minutes	Bubble size control for biomedical applications	90, 91
	Extraction force	Pressure difference between the outlet and gas flow channels	Air–water bubble	250 μm		The bubbles are generated for an elapsed time of 0.2604×10^{-3} s	Airborne particle collection	87
Acoustic	Acoustic radiation force	SAW and applied power is 400 mW	Vapor bubble	1–10 μm		The bubbles are aligned into multiple parallel lines	Bubble manipulation	92
	Acoustic pressure	Piezoelectric disk	Vapor bubble	—	Generate in an acoustically profiled microfluidic structure (low pressure regions)	The bubbles are removed when the flow rate is high	Mixing enhancement for highly viscous fluids	98
	Acoustic pressure	Ultrasonic transducer	Oil–water bubble	~41–67 μm (can be increased by turning on the transducer)	Forms at the cross junction of the microchannel	—	Bubble size control	99

volume and lifetime of the bubble depend on the laser wavelength, focal spot, laser fluence and pulse duration.[47] Several techniques implemented using pulsed lasers have been reported for bubble trapping in microfluidics. Ohl, C. D. et al. created a bubble near a solid surface.[48] The bubble close to a surface is created by an intense laser pulse from a Q-switched laser into a water-filled cuvette. The bubble dynamics revealed four stages: bubble expansion, bubble collapse, jetting and expansion, which will induce a shear flow to remove particles from the surface and realize local surface cleaning. Aside from creating bubbles near a surface, suspended bubbles can also be trapped in liquid. Recently, Wu et al. reported that a suspended bubble trapped in a microchannel triggered by a pulsed laser could be applied for fluorescence-activated cell sorting (PLACS).[47] With the aid of the pulsed laser, the suspended bubble expands and collapses in 30 μs. As shown in Fig. 2a, when the bubble expands and collapses, the fluid can be switched; with controlling the pulsed time interval, target fluorescent cells can be sorted efficiently. Using the same bubble trapping method, 3D PLACS was developed by thin-film PDMS fabrication techniques, which achieves a higher throughput than PLACS by studying the laser energy, nozzle shape, and bubble size.[49] Due to the advantage of precise location control, the pulsed laser was used to trap the bubble next to the cell. The collapse of bubbles will lead to microjetting, deforming and porating cell membranes (Fig. 2b).[50,51]

The continuous-wave (CW) laser, emitting a continuous laser beam with output heat control, is also applied in bubble trapping for microfluidics. Once the CW laser focuses on the liquid, the surrounding liquid is sufficiently heated to evaporation which forms a bubble at the center of the beam.

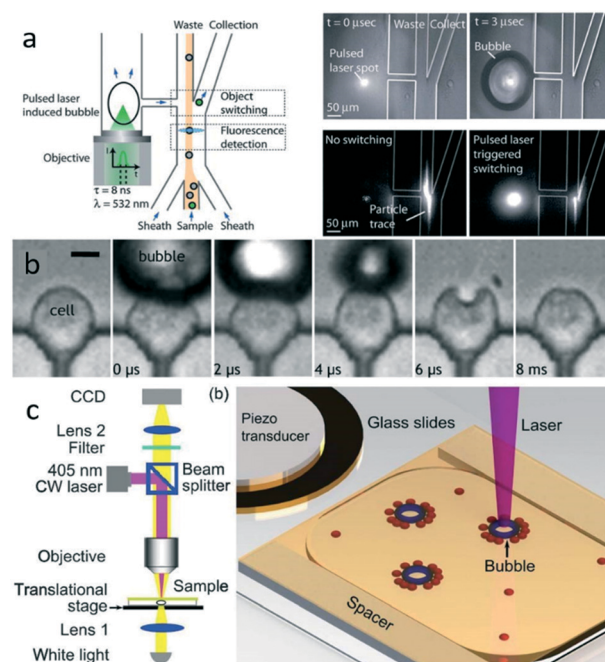**Fig. 2** (a) Schematic presentation of the bubble generation process by the focused laser beam and particle sorting in PLACS. Reprinted with permission from ref. 47. (b) Laser induced microbubble expansion and collapse for single-cell membrane poration. Reprinted with permission from ref. 50. (c) The setup of the laser system and the mechanism of generating bubbles. Reprinted with permission from ref. 58.

With the continuous laser power, the bubble will gradually grow and then achieve saturation at a size dominated by vaporization.[52] When the laser is turned off, the bubble shrinks and finally collapses.[53] By experimentally investigating the temporal evolution of CW-laser induced bubbles, Kim *et al.* provided the knowledge of predicting and controlling the bubble size for a long time duration.[54] Compared with the pulsed laser technique, the CW laser method can produce more stable bubbles that are suitable for long-period bubble-based microfluidic applications. For instance, Taylor, R. and C. Hnatovsky introduced a stable bubble generation technique by using a low power CW laser coupled into a fiber probe.[55] The stable bubbles were trapped at a submerged taped near-field scanning optical microscopy (NSOM) fiber tip in distilled water in the range of 40–400 μm, with a lifetime of over an hour. Zhang *et al.* reported an effective method to create bubbles with controllable sizes in a microchannel using a CW laser light shone onto different patterned chromium pads in various fluids.[52] By controlling the size of bubbles with adjustable laser power, bubbles can release cells from the capturing area. Namura *et al.* developed a microfluidic control method by integrating a CW induced bubble and gold nanoparticles.[56] Generated by CW power in a microfluidic chamber, the bubble was heated on a gold island film, which induced Marangoni flow around the bubble. When the CW laser power changes, the flow direction can be instantaneously switched in response to the laser power. Xie *et al.* utilized the acoustic field to actuate a CW laser created micro-sized bubble where the second radiation force was produced and applied to deform the cells[57] and concentrate the cells (Fig. 2c).[58] The size of the bubble can be controlled with adjustment of illuminating time and laser power.

The optical control technique allows the bubble to be trapped at any location of a microchannel and enables a flexible bubble size control. However, the stability of the bubble and complex experimental setups still need to be further improved. The applied high energy has the potential to impact the cell viability as well.

2.2 Thermal control

Thermal control is a widely used technique for trapping and controlling bubbles in microfluidics. Heated by a heating source, the water inside the microchannel is transferred from the liquid phase to the gas phase and then the thermal vapor bubble is generated in the desired position. With controlling heating sources, the bubble grows and finally collapses due to the condensation of the vapor at the bubble interface. Thermally induced bubbles have been employed as actuators, pumps, rotors and valves for microfluidic applications.[59–61] Among these thermal bubble based applications, different techniques are employed to form bubbles. A silicon microheater is the most common one that is used to create individual and controllable thermal bubbles in a microchannel. Using a heater with two embedded polysilicon lines, Jung *et al.* created a thermal bubble

in a microchamber.[62] In their works, a desired size of the bubble can be obtained when the heater size, chamber depth and pulse duration are matched well. Besides, the growth and collapse of bubbles induced a pumping flow, which can be controlled by the pulse duration and input pulse voltage. The thermal bubble induced by the embedded silicon microheater has also been applied to sort bioparticles[63,64] and separate single microparticles.[65] Different from the embedded silicon microheater, Tsou *et al.* proposed a silicon-based vertical microheater to generate thermal bubbles that attach to the sidewall of the microchannel.[66] With controlling the bubble size, this device is successfully employed in switching fluid and integrating with microfluidic systems. Apart from the silicon microheater, thermal bubbles can also be generated using a platinum microheater, which is more stable at high temperatures. For example, Wang *et al.* utilized a thin-film platinum microheater to trap and control bubbles within a high temperature range.[67] Due to the Marangoni effect, the liquid–vapor interface changed quickly and the heat transferred to the surrounding liquid, inducing the mixing effect in the microchannel. Qu *et al.* were able to trap a thermal vapor bubble in a microchannel for investigating the effect of acoustic force on the vapor bubble using a single platinum serpentine microheater.[68] Wang *et al.* patterned a superhydrophobic material copper surface to generate thermal bubbles, which can effectively lower the bubble formation temperature and facilitate bubble detachment.[69] Using resistors as the heat source, these above-mentioned techniques provide a controllable and stable way to generate bubbles in microfluidics. However, an associated drawback with the micro resistance heater is that the resister needs to be connected to an outer power supply, which increases the complexity of the system. This shortcoming was fixed by using induction heating technology to generate thermal bubbles without physical contact and an external power supply circuit.[70–72] Based on the principles of heat transfer and electromagnetic induction, the heating plate can transfer the power from the electromagnetic field and eddy current without contact. Liu *et al.* experimentally investigated the impact of the thickness of the heating plate on the induction heater for thermal bubble generation.[70] To generate thermal bubbles with minimum power, they experimentally determined the optimum thickness of the heating plate. The heat inducted thermal bubble can be used as the actuator in microfluidic applications based on explosive evaporation. Although the induction heating technology realizes non-contact heating, for portable microfluidic applications, the bulky power supply for generating bubbles still hinders the effort of miniaturization. The incubator was also applied as a heat source for increasing the bubble size inside the channel, but the unwanted bubble generation can be a potential issue.[73]

2.3 Electrical control

Electric fields can be employed to effectively trap bubbles in microfluidics. To apply the electrical energy, one or two pairs of electrodes are embedded in a microfluidic device and are

connected to an electrical power supply. The power supply can be divided into two types: alternating current (AC) electric field and direct current (DC) electric field. With the aid of an AC or DC field, bubbles can be trapped and controlled in microfluidic devices by electric force or an electrochemical reaction.

With the advantages of low energy requirement, the electrochemical technique is regarded as an effective way to trap bubbles in the microchannel. Fattah *et al.* introduced an electrochemical method for bubble generation using a modified carbon microtube (CMT).[74] Based on the concept of bipolar electrochemistry (BPE), an oxygen bubble is formed at one end with a Pt cluster of the CMT, which induces a local mechanical perturbation and movement of the CMT microswimmer in the opposite direction. The external electric field not only realizes the generation of bubbles at one side of the conducting object, but also enables the local generation of gas bubbles as both extremities of the object.[75] As a result of two redox reactions across bipolar electrodes, various amounts of H_2 bubbles and O_2 bubbles can be generated at different sides of bipolar electrodes in pure water, when the amplitude of the electrical field is chosen above a given threshold. Moreover, the unbalanced quantity of H_2 and O_2 bubbles can induce the motion of the bipolar electrodes and thus can be further exploited for electrode motion control (Fig. 3a).[76] To further understand the electrochemical reaction, Li *et al.* investigated the evolution of the H_2 and O_2 bubbles generated by the electrochemical reaction in a microchannel filled with water. They found that the diameter of bubbles is proportional to the current density, but is inversely proportional to the flow velocity.[77] Using the electrochemical technique, Ma *et al.* successfully generated programmable on-demand H_2 and O_2 bubble patterns at gold and copper electrodes (Fig. 3c).[78] The size of the bubble was defined by controlling the current. Due to the acoustic impedance difference between gas and liquid, these bubbles can effectively block ultrasound. By digitally controlling the bubble patterns, they realized spatial ultrasound modulation.

Compared with thermally trapped bubbles, electrochemical bubbles require lower energy input but are limited by slow bubble deflation rates. Using a picomole of salt, Hua *et al.*

successfully produced an H_2 electrochemical bubble in a microchannel and applied it as a valve that can open and close in milliseconds by voltage pulse.[31] They found that bubble deflation rates increased with the decrease of the dimension of the microchannel, while bubble inflation rates increased with the increase of the input voltage. With electrolysis of water, Obata *et al.* trapped a hydrogen bubble on a platinum electrode and controlled the bubble *via* adjusting the mixing potential.[79] By controlling the generation and shrinkage of the electrochemical bubble, the bi-directional movement of the fluid in a microchannel was realized.

Different from electrochemically generated bubbles, using a pair of electrodes, a vapor bubble can be generated inside a microchannel by sparks. Specifically, when a high voltage spark discharge is applied to the electrodes, an electric break down of dielectric liquid is created between the electrodes, which induces a localized plasma and forms the bubble by vaporization. By integrating the spark induced vapor bubble into a microchannel, a high-speed and accurate cell sorter was realized.[80] With the expansion of the bubble, the sample is pushed away to the collection channel; in the bubble collapse period, the stream flows back to the waste channel. Besides, the sorting performance can be optimized with testing different voltages and pulse durations. Since the generation and collapse of a bubble can generate vortices, the high voltage pulse induced bubbles were also applied to mix the fluid (Fig. 3b).[81]

2.4 Mechanical control

Mechanical bubble trapping and control techniques are usually implemented by integrating a microfluidic device with an external gas or vacuum supply. When gas is injected into a microchannel filled with liquid, gas pressure can be controlled with the flow rates of gas.[82] As an example, using a syringe pump, gas is periodically injected into the liquid channel to create bubbles.[83–85] With ultrasonic exposure, the gas–liquid interfaces in the microchannel are able to completely lyse bacteria and yeast cells within one second. Bubbles can also be mechanically controlled by hydrodynamic actuation. Khoshmanesh *et al.* drew an air bubble at the tip of a feeder
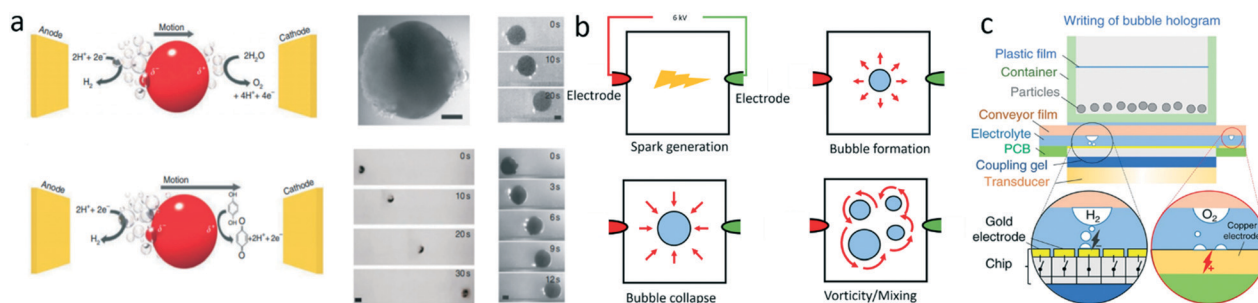
Fig. 3 (a) O_2 and H_2 bubble generation and bubble induced transition motion of an object by bipolar electrochemistry. Reprinted with permission from ref. 76. (b) The high-voltage pulse between two electrodes induces an electric spark for bubble formation and its application of mixing fluid.[81] (c). Programmable on-demand H_2 and O_2 bubbles are generated on gold and copper electrodes by the electrochemical method. Reprinted with permission from ref. 78.

tube and moved it along a feeder channel.[86] Under the hydrodynamic actuation, the oscillating bubble inside the feeder channel induces a strong disturbance in the main channel and thus enhances the mixing efficiency. Using a stepper motor, the size and shape of the bubble were precisely controlled by adjusting the gas pressure. Thus, the application of particle patterning in the main channel was realized (Fig. 4a). Bubbles were effectively produced by continually driving air through a microchannel array. Because of the pressure difference between gas supply channels and the outlet of the reservoirs, bubbles were generated at the end of gas supply channels. When bubbles are formed, the particles were trapped inside the bubbles and released into a liquid reservoir with 90% collection efficiency. Additionally, a Teflon layer was coated on the microchannel walls which will increase the hydrophobicity of the microchannels and result in stable and continuous bubbles.[87]

Apart from gas injection, pressure has been used to control the bubble size and position as well. Liu *et al.* introduced a microfluidic standing air bubble system which consists of a bubble channel, pneumatic channels, and permeable porous barriers between them.[88] The size of the bubble can be controlled by adjusting the pneumatic pressure (−90 kPa to 200 kPa). This study introduced a way not only to control the bubble size, but also to enhance the stability of bubbles by the control of air diffusion between pneumatic channels and bubbles. Using a similar method, the control of bubble position was also realized and applied in tuning the concentration gradient of a solution.[89] Under various vacuum pressures, the size of the bubble can be controlled for different applications. By applying the above mentioned approach, researchers shrank bubbles in microchannels as small as sub-micrometer diameters by embedding a vacuum channel on the microfluidics device (Fig. 4b),[90,91] which provides an effective way for users to engineer a desired bubble size in microfluidic platforms.

2.5 Acoustic control

Acoustic control is a powerful way to trap and manipulate bubbles in microfluidic applications, which can be categorized into two types: surface acoustic wave (SAW) based acoustic actuation and bulk acoustic wave (BAW) based acoustic actuation. For the former type, the transducer will generate acoustic waves that propagate along the surface and it generally operates at high frequencies. For the latter type, the piezoelectric transducer is widely used to produce the acoustic waves that propagate in the direction perpendicular to the surface.

Bubbles can be trapped and controlled by SAW for microfluidic applications. SAW was used to induce bubbles in a 3D microfluidic device to selectively trap and on-demand release droplets in the microchannel. With controlling the position of acoustic actuation, the individual droplets were selectively manipulated and released based on the demand. SAW is also employed in manipulating bubbles. For example, SAW was used to align and trap bubbles in a microfluidic device with different heights of microcavities.[92] If the height of the cavity is smaller than the wavelength of the SAW, bubbles can be aligned into parallel lines inside the microchamber which is dominated by acoustic radiation force; meanwhile when the height of the cavity is larger than the wavelength of the SAW, acoustic streaming will dominate. Thus, the bubble can be trapped in the center of the microcavity by adjusting the height of the cavity. It is also found that the trapping rate increases with increasing input power and decreasing flow rate.

Different from SAW, BAW is generated by a piezoelectric transducer, which is operated at relatively low frequencies and can be placed on the bottom, sidewall and top of the microfluidic device. Wang *et al.* introduced a method to generate a bubble in a microfluidic channel for mixing enhancement with the actuation of a piezoelectric disk in an effective frequency range.[100] It is found that the bubble can be generated inside the actuation chamber because there is a low-pressure region where the water pressure is lower than the vapor pressure. Using the same mechanism, an acoustically generated bubble was successfully utilized to mix highly viscous fluid (DI water and glycerol solutions) with viscosity up to 44.75 mPa s in microfluidic systems (Fig. 5a).[98] An acoustic transducer is also employed in controlling the size of bubbles. Chong *et al.* reported a method to control the size of bubbles in acoustofluidic devices.[99] Using an ultrasonic transducer, they induced microstreaming around the bubble, which affects the gas bubble formation by increasing the gas flow rate (Fig. 5b).
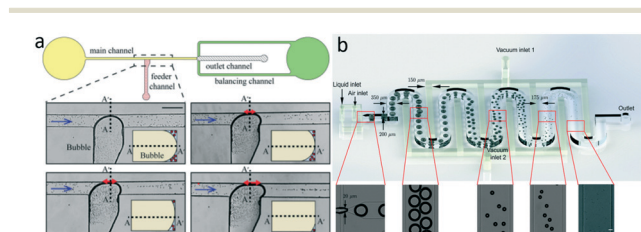
Fig. 4 (a) The application of patterning particles by controlling the shape and size of the bubble with a stepper motor. Reprinted with permission from ref. 86. (b) The sequential shrinking of bubbles by applying vacuum pressure. Reprinted with permission from ref. 91.
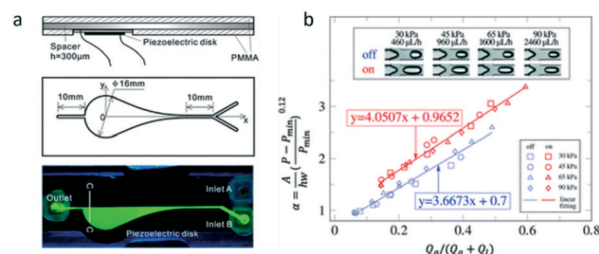
Fig. 5 (a) Side view and top view of the acoustically induced bubble based micro mixer. Reprinted with permission from ref. 98. (b) Under different flow conditions, the bubble size in dimensionless number changed with and without acoustic actuation. Reprinted with permission from ref. 99.

The test result shows that various bubble sizes can be controlled with different actuation frequencies. In addition, at a fixed frequency, the size of the bubble is proportional to the input power through the transducer.

3. Passive trapping and control techniques

Unlike active techniques, passive trapping and control techniques do not require external energy, thus providing an alternative approach with advantages of being simple, low cost and energy saving. Based on fluid and surface properties, the geometries and properties of the microchannels can be designed and modified to trap the bubble in a desired position and size. The passively trapped bubbles have been widely applied in various microfluidic applications with actuation of external fields, such as an acoustic field and electric field. In this section, the passive bubble trapping and control techniques are introduced from two categories: device geometry and surface properties (Table 2).

3.1 Device geometry

Based on theoretical and experimental results, microcavities and microchannels have been successfully applied to trap bubbles with various shapes, positions, and sizes. According to the functional requirements, various types of bubbles, such as hemicylindrical air bubbles and hemispherical air bubbles, have been trapped and employed as micromixers, micropumps, microswimmers, microvalves, microrobots, etc. The following parts give an overview of the design of device geometry for trapping and controlling bubbles together with their applications in microfluidics.

In microfluidics, fluid flow is generally in the low Reynold's number range. When the fluid passes the pre-designed microcavity, air can be trapped in the microcavity

and the air–liquid interface is passively formed. Here, we present advanced bubble trapping methods using microcavities with different geometries as well as related microfluidic applications.

3.1.1 Single layer microcavity. Single layer microcavity, which can be simply fabricated by photolithography or micromilling technology, is widely applied to trap the bubble in different locations of the microfluidic channel. Three types of single layer cavities have been used to trap the bubble on the side wall: vertical cavity,[101] lateral cavity,[14] and triangle cavity.[88] These cavities are designed at one or two sides of the microchannel, which can trap air bubbles when the microchannel is filled with liquid. Vertical rectangular cavities are designed to trap hemicylindrical bubbles. Under acoustic actuation, the oscillating hemicylindrical bubble would induce symmetric microstreaming flow around, which is capable of mixing the fluid in the microchannel,[101] and manipulate cells, particles and microorganisms (Fig. 6a).[102,103] Different from vertical cavities, lateral cavities are able to trap asymmetric hemispherical shaped air bubbles, which would generate a directional microstreaming flow under acoustic excitation and could be applied in pumping particles, enriching and sorting cellular subsets from whole blood (Fig. 6b).[14,19]

Besides creating the cavity at the end side of the microchannel, the cavity can also be designed inside the microchannel with high flexibility. Ahmed et al. trapped a single bubble by a "horse-shoe" shaped microcavity located between two laminar flows inside a microchannel.[104] When applying the acoustic wave, the trapped bubble disrupts the two laminar flows and mixes the fluids in milliseconds. The multiple "horse-shoe" shaped microcavities were developed to trap bubbles inside a microchannel with precise control of location and size.[105] By turning on/off the acoustic wave, multiple bubbles are capable of controlling the particle trajectory in a wide range. Using a similar structure, our group oppositely placed two different sized cavity structures

Table 2 Comparison of different passive bubble trapping and control techniques

| Technique		Type of bubble	Size of bubble (diameter)	Location of bubble	Performance	Application	Ref.
Device geometry	Single layer microcavity	Air–water bubble	41 μm, 90 μm, 100 μm, 120 μm and 320 μm (controlled by the dimension of the cavity)	Bubbles are trapped on the sidewall, center and substrate of the microchannel (determined by the location of cavity structures)	Cavity structures protect bubbles from dissolving and the lifetime can be prolonged for hours	Cell separation, cell enrichment, micromixer, micropump	19, 101, 104, 106
	3D microcavity	Air–water bubble	14.55 μm, 15 μm and 20 μm,			Micromixer, micropump, micropropulsor	16, 110, 111
	Mobile cavity	Air–water bubble	9 μm, 20 μm			Microswimmer, microrobot	43, 114
Surface properties	Chemical treatment	Air–water bubble/air–oil bubble	250 μm, 300 μm, 400 μm	Bubbles are trapped on the treated surfaces	Chemical treatment improves the stability of bubbles	Micropump	120
	Physical treatment	Air–water bubble	20 μm (controlled by the size of the micro/nano structure)	Bubbles are trapped on or between micro/nano structures	Decreasing the size of the structures enhances bubble stability	Micromixer, drag reduction	38, 125
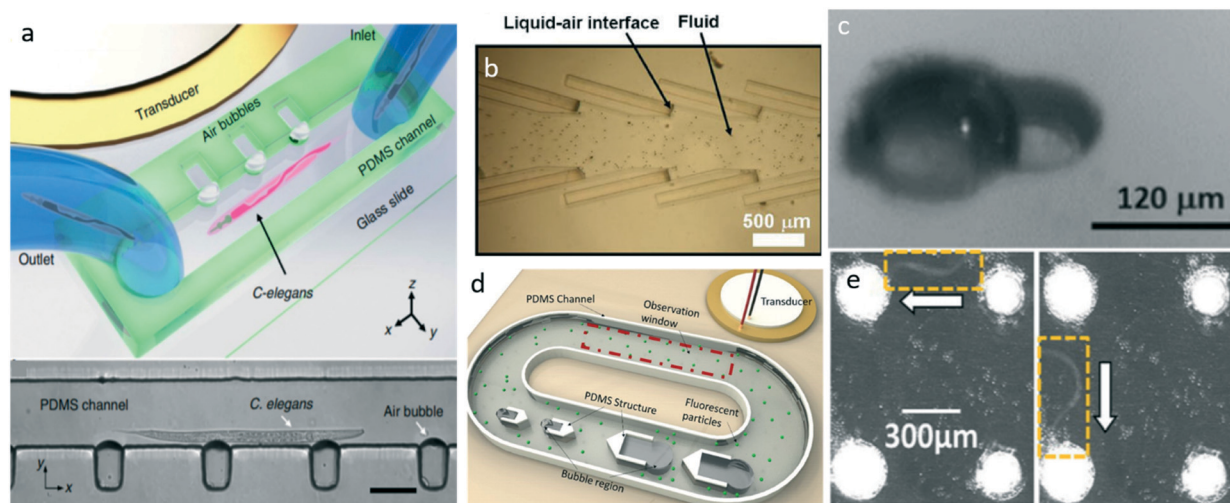
Fig. 6 (a) Schematic illustration of bubbles trapped in vertical cavities. Reprinted with permission from ref. 103. (b) Lateral cavity generated bubbles for pumping fluids. Reprinted with permission from ref. 14. (c) Teardrop shaped microcavity trapped microbubble on the substrate. Reprinted with permission from ref. 37. (d) Different sized bubbles trapped by a single layer microcavity structure for a bi-directional micropump. Reprinted with permission from ref. 106. (e) A microbubble array trapped on the bottom of the channel for manipulating *C. elegans*. Reprinted with permission from ref. 108.

to trap bubbles in the center of a recirculated microchannel (Fig. 6d).[106] By tuning the input frequency, the direction of microstreaming flow generated by oscillating bubbles is switched, which can be employed in bi-directional cells or particle transportation.

Apart from the above-mentioned cylindrical shaped bubble, a passively trapped spherical shaped bubble is also commonly investigated and applied in various microfluidic applications. To study the dynamics of the entrapped bubble under ultrasonic irradiation, spherical bubbles were successfully trapped by the cylindrical cavities etched in silicon and glass substrates.[107] Hashmi *et al.* introduced a way to trap bubbles by teardrop bottom cavities with the use of a micromilling machine (Fig. 6c).[37] With acoustic actuation, these entrapped bubbles in teardrop cavities generated a directional microstreaming flow, which can be further employed in drug delivery systems. To obtain a bubble array at the bottom of the channel, our group created an array of micrometer-sized holes to passively trap the air bubble.[108] The size and location of bubbles can be determined by the size and location of the cavities. Using acoustic radiation force, the oscillating bubble array is used to trap and enrich the microorganism (*Caenorhabditis elegans*), as demonstrated in Fig. 6e. A cylindrical microcavity array has also been fabricated on four PMMA plates, which are vertically fixed inside a microchamber and above a nanosensor.[109] When applying the resonant frequency to the device, the bubble arrays oscillate and generate microstreaming flow to enhance the mixing effect, resulting in a drastic reduction of sensing time.

3.1.2 3D microcavity structure. With the development of 3D printing technology, the sub-micron fabrication technique has been utilized for precisely producing micrometer sized 3D structures. Using a two-photon absorption microscopy

device, Bertin *et al.* fabricated hollow capsules as propulsors to trap spherical bubbles with different predetermined patterns and directions.[16] Excited by acoustic waves, various micro streaming flow patterns are generated in free space based on the arrangement of the capsules, as shown in Fig. 7a. Instead of creating a 3D structure in free space, our group introduced a flexible bubble trapping technique by integrating defended oscillating membrane equipped
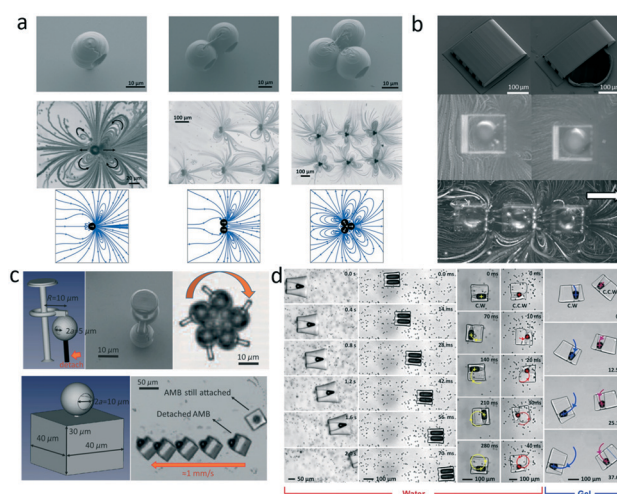
Fig. 7 (a) 3D printed microcavity structures and microstreaming patterns generated by the trapped bubbles. Reprinted with permission from ref. 16. (b) SEM image of the DOMES structure for bubble trapping and directional microstreaming flow around the trapped bubble. Reprinted with permission from ref. 111. (c) Schematic illustration of the armored microbubble swimmer and the motion induced by acoustic energy. Reprinted with permission from ref. 43. (d) Selective manipulation of bubble-based microswimmers in water and gel by adjusting the applied frequency. Reprinted with permission from ref. 113.

structures (DOMES) with the microchannel.[110,111] The DOMES structure is fabricated on a flexible PET substrate by two-photon polymerization, and then combined with a PDMS channel and double-sided tape by manual alignment. When the fluid flows through the structure, the spherical air bubbles can be passively trapped by the cavity of the 3D structure (Fig. 7b). Under the structure, a through-hole connects to the atmosphere, which increases the stability of bubbles and extends their lifetime. With different cavity patterns and sizes, the DOMES device is capable of mixing and pumping fluid by the acoustic driven bubbles. These above-mentioned methods demonstrated the contributions of 3D cavity structures in protecting bubbles and maintaining bubbles. Although the mass production of the structure is limited by the expensive fabrication costs, the flexible 3D microcavity structure shows great potential in various bubble-based applications in future.

3.1.3 Mobile cavity structure. Bubbles can be trapped in a mobile cavity structure and controlled by external fields as a microswimmer, which presents great promise for moving and transporting objects in microfluidic applications. Using 3D microfabrication, Bertin *et al.* created a free cavity structure to trap 3D microbubbles, called armored microbubbles (AMBs).[43] When the structure is submerged in liquid, the AMBs can be trapped in the shape of the hollow capsule. Unlike free bubbles in water, the bubbles can be protected from dissolution by the cavity structure and their lifetime can be prolonged for hours. By applying acoustic waves, AMBs can be propelled by the streaming flow around, as shown in Fig. 7c. With the use of microlithography, Feng *et al.* produced several end open microchannels to trap bubbles by simply submerging the channel in liquid.[112] In their work, the bubble size is determined by the dimension of the microchannel. Using this bubble trapping method, they trapped a single bubble, an array of bubbles and embedded bubbles in a turbo blade, respectively. When the input frequency is well tuned, the oscillating single bubble and the array of bubbles are able to propel the objects; the bubbles embedded in a turbo blade can generate torque and rotate the swimmer.

Using photopolymerization, another type of acoustic microswimmer that consists of a rectangular polymer body with several conical indentations was created.[113] The indentations of the structure were used to trap bubbles inside when the microswimmer was submerged in a chamber filled with liquid. Moreover, the diameter and depth of the indentations can control the bubble's motion. Since the resonant frequency depends on the size and shape of bubbles, the oscillation motion of bubbles can be activated by changing the frequency. Therefore, by controlling the size and shape of trapped bubbles, selective actuation of a single microswimmer then was realized (Fig. 7d).[113] Using a similar fabrication method, a microrobot with an inner spherical body cavity was created to trap a spherical air bubble.[114] With the control of acoustic and magnetic fields, the motion direction control

of the microrobots inside the microchannel has been tested, showing great promise in biomedical applications. Moreover, 3D direct laser lithography was also employed in creating movable 3D cavity structures for bubble trapping.[115]

3.1.4 Microchannel geometry. Passive bubble trapping is also realized by utilizing the geometry of the microchannel, such as corner, dead end or some special structures inside the microchannel. Due to surface tension, bubbles can be inevitably trapped at specific positions inside microchannels. By utilizing structures of the microchannel, researchers are able to use bubbles based on the need of microfluidic applications.

Bubbles trapped in corners are usually undesired for most applications. However, it is possible to utilize these undesired bubbles if there are some techniques to control them. For this phenomenon, Liu *et al.* studied the growth of air bubbles during negative pressure driven flow in the corner of a PDMS channel (Fig. 8b).[116] From the simulated and experimental results, they found that the growth rate of bubbles is quantitatively correlated to the bubble's location and driving pressure, which provides the strategy to control the bubble in bubble-based applications. Aside from the corner, the structure inside the microchannel is also applied for bubble trapping.[117] A square shaped bubble trap structure was created inside a microchannel to effectively trap a bubble using the curvature effects from the Young–Laplace equation. In this work, an offset region was created to detach the bubble from the upper wall. Once the bubble was detached from the wall, the flow would drive the bubble toward the trap region. By applying offset regions with different lengths, the trap can hold different sized bubbles (Fig. 8a). This method could be utilized in trapping bubbles at desired locations based on the requirements of applications. It is also found that bubbles can be passively trapped at the top of the cylindrical and hemispherical well in the microchannel.[118,119] When a bubble flows through the bubble trapping chamber,
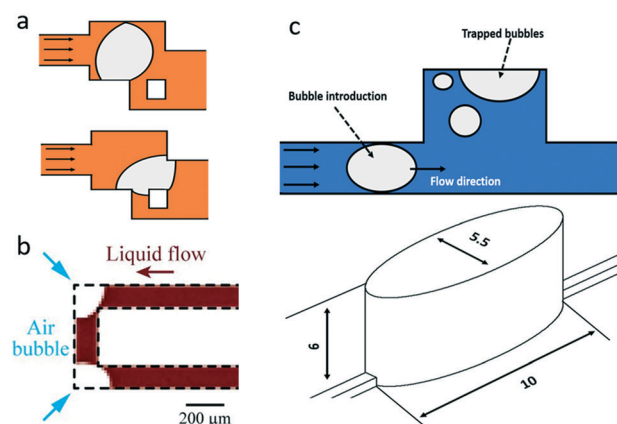
Fig. 8 (a) Design of a microchannel structure for trapping bubbles.[117] (b) Bubbles trapped at the square corner of the microchannel. Reprinted with permission from ref. 116. (c) Bubbles trapped at the top of a cylindrical chamber in the microchannel.[118]

the bubble will rise to the top of the chamber due to buoyancy (Fig. 8c). When the rising velocity (v_{rising}) is larger than the flow velocity (v), the bubble will float and attach to the top wall. Thus, the dimension of the well can be determined by controlling the rising velocity, which is expressed in eqn (4).

$$v_{rising} = \frac{g\Delta\rho d_b}{18\mu} \tag{2}$$

$$v = \frac{Q}{A} \tag{3}$$

$$d_b > \frac{18\mu Q}{g\Delta\rho A} \tag{4}$$

where g denotes the acceleration of gravity, $\Delta\rho$ is the density difference between bubbles and surrounding liquid, d_b is the diameter of bubbles, μ is the viscosity of the surrounding liquid, Q is the flow rate and A is the cross-section area of the channel.[118]

3.2 Surface properties

Surface properties, such as wettability, adhesiveness, capillarity, and surface tension, have significant impacts on bubble trapping and control. Among these surface properties, the wettability of a surface can be controlled by modifying the chemical composition and/or roughness of the surface. Here, we summarize the techniques for effectively trapping and controlling bubbles *via* modifying surface properties.

3.2.1 Chemical treatment. Chemical coating is regarded as a one-step method to modify the surface properties for bubble trapping and control. Depositing specific chemical agents on a surface can reduced surface energy and thus improve the surface hydrophobicity. Hence, bubbles are easier to be trapped on the surface and their stability is enhanced. Perfluorodecyltrichlorosilane (FDTS) is a chemical solution that can lower surface energy. By treating the surface

of the sidewall with FDTS *via* vapor deposition, the contact angle of oil on the FDTS treated surface was larger than 90 degrees and thus the air–oil bubbles can be perfectly trapped and maintained on the treated sidewall for half an hour (Fig. 9a).[120] With acoustic actuation, the trapped air/oil interfaces can generate a directional pumping flow in an oil liquid. Moreover, the stability of bubbles can be improved by depositing a chemical layer. For instance, a hydrophobic Cytop layer was deposited on the surface where the bubble is placed, which improves the adhesion of the bubble and eliminates random bubble motions under acoustic excitation.[121] By coating a cylindrical cavity with Rain-X, a superhydrophobic surface applied product, Chen *et al.* successfully created and stabilized bubbles.[122]

The polytetrafluoroethylene (PTFE) surface, also called the Teflon surface, is hydrophobic in air and hydrophilic in water, which is applied to trap air bubbles. Interestingly, using vacuum treatment, the treated surface of the sample can become superhydrophobic in water.[123] Once the sample was dried and immersed in water, the PTFE surface will be recovered, resulting in the sample becoming hydrophilic underwater. The round-trip transition can trap the bubble with a certain location as well as control the path of the bubble through the PTFE surface. Additionally, by means of the above-mentioned method, the underwater bubble can be switchable for many times (Fig. 9c). By spin coating the PTFE on the nanostructure surface, two water–air interfaces were created and applied in guiding waves for optofluidics.[124]

3.2.2 Physical treatment. Increasing the roughness will enhance the hydrophobic behavior, and thus enhance the bubble trapping efficiency. Many biological surfaces, such as plant leaves, have high surface roughness with the geometrical microstructure to repel water for cleaning and transporting nutrition. Based on the same principle, geometrical micro/nanostructures are studied to increase the roughness for trapping the bubble. For example, a rough wavy structure of a PDMS channel sidewall was made for capturing bubbles inside the microchannel, fabricated by the
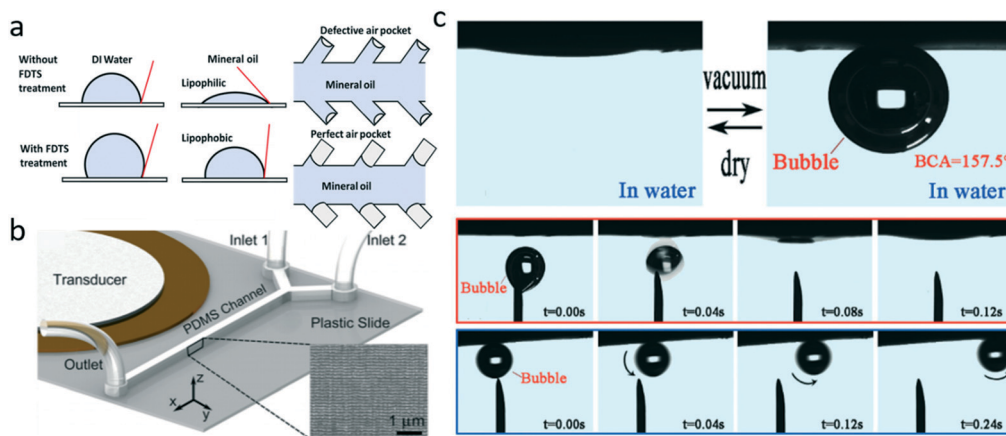
Fig. 9 (a) Difference in the performance of bubble trapping without and with FDTS treatment.[120] (b) Schematic illustration of a wavy PDMS structure in the microchannel for capturing bubbles. Reprinted with permission from ref. 125. (c) The transformation of a hydrophilic surface to a hydrophobic one for bubbles on a laser induced rough PTFE surface with vacuum and dry treatments. Reprinted with permission from ref. 123.

deep reactive ion etching (DRIE) process.[125] Since the wavy structure has a rough surface, the hydrophobicity of the PDMS sidewall is enhanced, resulting in the air bubble being trapped on the wavy structure. The bubble in the presence of acoustic waves was used for rapidly mixing two viscous fluids, which could be integrated into various lab-on-a-chip applications (Fig. 9b). Similarly, a textured rough surface with nanostructures can also be effectively used to trap the bubble.[126] Moreover, by integrating a porous hydrophobic membrane with the microchannel, bubbles can be trapped and removed from the porous membrane area with the appropriate bubble length, time, flow rate and pressure difference. According to the theoretical and experimental results, once the bubble length, time, flow rate and pressure difference are satisfied at the same time, complete bubble extraction can be realized.[127]

Besides, many types of micro/nano structure patterns with hydrophobic surfaces, such as ridges,[128] trenches,[129] pillars,[130] and irregular structures,[131] have been applied to trap bubbles (air–liquid interfaces) for drag reduction in laminar flows. Supported by surface tension, the air–liquid interface between structures is shear free and does not resist flow.[132] Therefore, drag is reduced due to the decreased surface area of the solid that is in contact with the fluid flow. Many theoretical predictions and experimental studies proved that the laminar drag can be significantly reduced using this technique.[133] However, the instability of the air–liquid interfaces could hinder the performance in practical applications. To address this issue, Choi et al. studied the effects of the pressure gradient on stability. They found that ridges with small width and length can enhance the stability of bubbles and the drag reduction efficiency even at a high pressure gradient.[38]

4. Conclusions

In the past few decades, as a promising tool, microbubbles have been applied in various microfluidic applications due to the advantages of cleanliness, flexibility and controllability. In this review, we summarized the active and passive trapping and control methods of bubbles in various microfluidic applications. With the help of external fields, such as optic, acoustic and electric fields, bubbles can be actively trapped at desired locations. Moreover, depending on the types of applications, tuning of energy input can control the size of bubbles. We also present a variety of passive bubble trapping and control methods based on modifying the device geometries and surface properties. From the former, based on the type and location of bubbles, we introduced many types of microcavities, microchannels for bubble trapping and control with novel fabrication techniques. The latter includes the techniques to form and manipulate bubbles by means of modifying the surface properties both physically and chemically. Additionally, by applying external forces (e.g. acoustic force), applications of these trapped bubbles have been extended to many fields, such as fluid control (mixing, pumping and switching), micro object manipulation (microorganism manipulation, cell lysis and cell separation) and mass transfer (drug delivery, microswimmer). Microbubbles have also been widely applied for drag reduction in microchannels, which could be helpful for reducing energy consumption in an engineered system. Despite these benefits, some of the issues remain to be further studied for trapping and control in bubble-based applications: the stability of bubbles and the undesired bubbles trapped in the microfluidic system. Although there exist some methods that offer the solution for stability enhancement such as changing the type of liquid, using a less soluble gas as the inner gas of the bubble and utilizing a surfactant to protect the bubble, the stability under different conditions is still challenging. In future, with more advanced theoretical and experimental developments of bubble trapping and control techniques, we believe that microbubbles will play more important roles in microfluidic applications, and solve challenging problems in many scientific and engineering fields.

Conflicts of interest

There are no conflicts to declare.

Acknowledgements

References

1 A. Prosperetti, Phys. Fluids, 2004, **16**, 1852–1865.
2 K. S. Suslick and G. J. Price, Annu. Rev. Mater. Sci., 1999, **29**, 295–326.
3 B. C. Donose, E. Taran, M. A. Hampton, S. I. Karakashev and A. V. Nguyen, Adv. Powder Technol., 2009, **20**, 257–261.
4 T. Georgiou, L. Britnell, P. Blake, R. V. Gorbachev, A. Gholinia, A. K. Geim, C. Casiraghi and K. S. Novoselov, Appl. Phys. Lett., 2011, **99**, 093103.
5 I. Leifer and I. MacDonald, Earth Planet. Sci. Lett., 2003, **210**, 411–424.
6 A. Patist and D. Bates, Innovative Food Sci. Emerging Technol., 2008, **9**, 147–154.
7 P. J. Cullen, Food mixing: Principles and applications, John Wiley & Sons, 2009.
8 R. Lavrijsen, D. M. F. Hartmann, A. van den Brink, Y. Yin, B. Barcones, R. A. Duine, M. A. Verheijen, H. J. M. Swagten and B. Koopmans, Phys. Rev. B: Condens. Matter Mater. Phys., 2015, **91**, 104414.
9 R. Bekeredjian, P. A. Grayburn and R. V. Shohet, J. Am. Coll. Cardiol., 2005, **45**, 329–335.
10 M. Postema and A. Bouakaz, Appl. Acoust., 2018, **140**, 150–152.
11 P. Voci, J. Am. Coll. Cardiol., 2000, **36**, 625–627.
12 A. Hashmi, G. Yu, M. Reilly-Collette, G. Heiman and J. Xu, Lab Chip, 2012, **12**, 4216–4227.
13 K. Ryu, S. K. Chung and S. K. Cho, JALA, 2010, **15**, 163–171.

14 A. R. Tovar, M. V. Patel and A. P. Lee, *Microfluid. Nanofluid.*, 2011, **10**, 1269–1278.

15 P. Rogers and A. Neild, *Lab Chip*, 2011, **11**, 3710–3715.

16 N. Bertin, T. A. Spelman, T. Combriat, H. Hue, O. Stephan, E. Lauga and P. Marmottant, *Lab Chip*, 2017, **17**, 1515–1528.

17 L. G. Dai, N. D. Jiao, X. D. Wang and L. Q. Liu, *Micromachines*, 2017, **8**, 130.

18 J. H. Shin, J. Seo, J. Hong and S. K. Chung, *Sens. Actuators, B*, 2017, **246**, 415–420.

19 N. Garg, T. M. Westerhof, V. Liu, R. Liu, E. L. Nelson and A. P. Lee, *Microsyst. Nanoeng.*, 2018, **4**, 1–9.

20 K. Kooiman, H. J. Vos, M. Versluis and N. de Jong, *Adv. Drug Delivery Rev.*, 2014, **72**, 28–48.

21 A. Kheirolomoom, P. A. Dayton, A. F. H. Lum, E. Little, E. E. Paoli, H. R. Zheng and K. W. Ferrara, *J. Controlled Release*, 2007, **118**, 275–284.

22 M. Ren, W. L. Guo, H. S. Guo and X. H. Ren, *ACS Appl. Mater. Interfaces*, 2019, **11**, 22761–22767.

23 W. Lauterborn and T. Kurz, *Rep. Prog. Phys.*, 2010, **73**, 106501.

24 T. T. Fu and Y. G. Ma, *Chem. Eng. Sci.*, 2015, **135**, 343–372.

25 W. Lauterborn, *J. Acoust. Soc. Am.*, 1976, **59**, 283–293.

26 R. Bolanos-Jimenez, M. Rossi, D. F. Rivas, C. J. Kahler and A. Marin, *J. Fluid Mech.*, 2017, **820**, 529–548.

27 N. Riley, *Annu. Rev. Fluid Mech.*, 2001, **33**, 43–65.

28 P. Marmottant and S. Hilgenfeldt, *Nature*, 2003, **423**, 153–156.

29 C. C. Coussios and R. A. Roy, *Annu. Rev. Fluid Mech.*, 2008, **40**, 395–420.

30 G. Yang, J.-J. Zhu, K. Okitsu, Y. Mizukoshi, B. M. Teo, N. Enomoto, S. G. Babu, B. Neppolian, M. Ashokkumar and S. Shaik, *Handbook of ultrasonics and sonochemistry*, Springer, 2016.

31 S. Z. Hua, F. Sachs, D. X. Yang and H. D. Chopra, *Anal. Chem.*, 2002, **74**, 6392–6396.

32 J. B. Wang, M. Sullivan and S. Z. Hua, *J. Microelectromech. Syst.*, 2007, **16**, 1087–1094.

33 S. S. Wang, X. Y. Huang and C. Yang, *J. Heat Transfer*, 2012, **134**, 051014.

34 A. N. Hellman, K. R. Rau, H. H. Yoon, S. Bae, J. F. Palmer, K. S. Phillips, N. L. Allbritton and V. Venugopalan, *Anal. Chem.*, 2007, **79**, 4484–4492.

35 L. Dai, N. Jiao and L. Liu, Particle manipulation via opto-thermally generated bubbles in open chip environment, *2016 IEEE 16th International Conference on Nanotechnology (IEEE-NANO)*, 2016, pp. 30–33.

36 H. B. Cheng and Y. W. Lu, *Microfluid. Nanofluid.*, 2014, **17**, 855–862.

37 A. Hashmi, G. Heiman, G. Yu, M. Lewis, H. J. Kwon and J. Xu, *Microfluid. Nanofluid.*, 2013, **14**, 591–596.

38 W. Choi, H. Byeon, J. Y. Park, I. C. Kim and S. J. Lee, *Appl. Phys. Lett.*, 2019, **114**, 101603.

39 P. Lv, Y. Xue, Y. Shi, H. Lin and H. Duan, *Phys. Rev. Lett.*, 2014, **112**, 196101.

40 E. Bormashenko, R. Pogreb, G. Whyman and M. Erlich, *Langmuir*, 2007, **23**, 6501–6503.

41 S. Poulain, E. Villermaux and L. Bourouiba, *J. Fluid Mech.*, 2018, **851**, 636–671.

42 A. B. Subramaniam, C. Mejean, M. Abkarian and H. A. Stone, *Langmuir*, 2006, **22**, 5986–5990.

43 N. Bertin, T. A. Spelman, O. Stephan, L. Gredy, M. Bouriau, E. Lauga and P. Marmottant, *Phys. Rev. Appl.*, 2015, **4**, 064012.

44 M. Lee, E. Y. Lee, D. Lee and B. J. Park, *Soft Matter*, 2015, **11**, 2067–2079.

45 K. W. Pulsipher, D. A. Hammer, D. Lee and C. M. Sehgal, *Ultrasound Med. Biol.*, 2018, **44**, 2441–2460.

46 J. Rodriguez-Rodriguez, A. Sevilla, C. Martinez-Bazan and J. M. Gordillo, *Annu. Rev. Fluid Mech.*, 2015, **47**, 405–429.

47 T.-H. Wu, Y. Chen, S.-Y. Park, J. Hong, T. Teslaa, J. F. Zhong, D. Di Carlo, M. A. Teitell and P.-Y. Chiou, *Lab Chip*, 2012, **12**, 1378–1383.

48 C. D. Ohl, M. Arora, R. Dijkink, V. Janve and D. Lohse, *Appl. Phys. Lett.*, 2006, **89**, 074102.

49 Y. Chen, T. H. Wu, Y. C. Kung, M. A. Teitell and P. Y. Chiou, *Analyst*, 2013, **138**, 7308–7315.

50 Z. Li, A. Liu, E. Klaseboer, J. Zhang and C. Ohl, *Lab Chip*, 2013, **13**, 1144–1150.

51 Q. Fan, W. Hu and A. T. Ohta, *Lab Chip*, 2014, **14**, 1572–1578.

52 K. Zhang, A. Q. Jian, X. M. Zhang, Y. Wang, Z. H. Li and H. Y. Tam, *Lab Chip*, 2011, **11**, 1389–1395.

53 W.-C. Shih, J. Li and F. Zhao, Holographic Microbubble Actuators for Microfluidic Manipulation and Particle Assembly, *2018 IEEE 18th International Conference on Nanotechnology (IEEE-NANO)*, 2018, pp. 1–4.

54 N. Kim, H. Park and H. Do, *Langmuir*, 2019, **35**, 3308–3318.

55 R. Taylor and C. Hnatovsky, *J. Appl. Phys.*, 2004, **95**, 8444–8449.

56 K. Namura, K. Nakajima, K. Kimura and M. Suzuki, *J. Nanophotonics*, 2016, **10**, 033006.

57 Y. L. Xie, N. Nama, P. Li, Z. M. Mao, P. H. Huang, C. L. Zhao, F. Costanzo and T. J. Huang, *Small*, 2016, **12**, 902–910.

58 Y. L. Xie, C. L. Zhao, Y. H. Zhao, S. X. Li, J. Rufo, S. K. Yang, F. Guo and T. J. Huang, *Lab Chip*, 2013, **13**, 1772–1779.

59 J. H. Tsai and L. W. Lin, *J. Microelectromech. Syst.*, 2002, **11**, 665–671.

60 X. P. Qu and H. H. Qiu, *J. Micromech. Microeng.*, 2010, **20**, 105015.

61 J. Kao, X. Wang, J. Warren, J. Xu and D. Attinger, *J. Micromech. Microeng.*, 2007, **17**, 2454.

62 J.-Y. Jung and H.-Y. Kwak, *Microfluid. Nanofluid.*, 2007, **3**, 161–169.

63 R. B. Maxwell, A. L. Gerhardt, M. Toner, M. L. Gray and M. A. Schmidt, *J. Microelectromech. Syst.*, 2003, **12**, 630–640.

64 C. C. Chen, J. S. Wang and O. Solgaard, *Sens. Actuators, B*, 2006, **117**, 523–529.

65 K. Tseng and C. F. Tsou, *Sens. Mater.*, 2014, **26**, 51–61.

66 C. F. Tsou and C. H. Huang, *J. Microelectromech. Syst.*, 2009, **18**, 852–859.

67 B. Wang, J. L. Xu, W. Zhang and Y. X. Li, *Sens. Actuators, A*, 2011, **169**, 194–205.

68 X. Qu and H. Qiu, *J. Micromech. Microeng.*, 2011, **21**, 105015.

69 X. Wang, S. Zhao, H. Wang and T. Pan, *Appl. Therm. Eng.*, 2012, **35**, 112–119.

70 B. D. Liu, Y. P. Hou, D. S. Li and J. H. Yang, *Sens. Actuators, A*, 2015, **222**, 8–14.

71 B. D. Liu, Y. P. Hou, J. C. Sun and J. H. Yang, *Microsyst. Technol.*, 2016, **22**, 1005–1011.

72 Y. P. Hou, B. D. Liu and J. H. Yang, *Microsyst. Technol.*, 2016, **22**, 103–108.

73 W. Xu, L. L. Wu, Y. Zhang, H. Xue, G. P. Li and M. Bachman, *Sens. Actuators, B*, 2009, **142**, 355–361.

74 Z. Fattah, G. Loget, V. Lapeyre, P. Garrigue, C. Warakulwit, J. Limtrakul, L. Bouffier and A. Kuhn, *Electrochim. Acta*, 2011, **56**, 10562–10566.

75 L. Bouffier, V. Ravaine, N. Sojic and A. Kuhn, *Curr. Opin. Colloid Interface Sci.*, 2016, **21**, 57–64.

76 G. Loget and A. Kuhn, *Nat. Commun.*, 2011, **2**, 535.

77 Y. F. Li, G. Q. Yang, S. L. Yu, Z. Y. Kang, J. K. Mo, B. Han, D. A. Talley and F. Y. Zhang, *Int. J. Hydrogen Energy*, 2019, **44**, 28283–28293.

78 Z. Ma, K. Melde, A. G. Athanassiadis, M. Schau, H. Richter, T. Qiu and P. Fischer, *Nat. Commun.*, 2020, **11**, 1–7.

79 H. Obata, T. Kuji, M. Yokokawa and H. Suzuki, Electrochemical bidirectional micropump for processing of liquid plugs, *2015 18th International Conference on Solid-State Sensors, Actuators and Microsystems (TRANSDUCERS)*, 2015, pp. 1786–1789.

80 J. J. Zhao and Z. You, *Cytometry, Part A*, 2018, **93**, 222–231.

81 S. Surdo, A. Diaspro and M. Duocastella, *Microfluid. Nanofluid.*, 2017, **21**, 82.

82 M. Johnson, G. Liddiard, M. Eddings and B. Gale, *J. Micromech. Microeng.*, 2009, **19**, 095011.

83 T. Tandiono, D. S. W. Ow, L. Driessen, C. S. H. Chin, E. Klaseboer, A. B. H. Choo, S. W. Ohl and C. D. Ohl, *Lab Chip*, 2012, **12**, 780–786.

84 J. Xu and D. Attinger, *J. Micromech. Microeng.*, 2007, **17**, 609.

85 J. Xu and D. Attinger, *Phys. Fluids*, 2007, **19**, 108107.

86 K. Khoshmanesh, A. Almansouri, H. Albloushi, P. Yi, R. Soffe and K. Kalantar-Zadeh, *Sci. Rep.*, 2015, **5**, 9942.

87 I. Mirzaee, M. Song, M. Charmchi and H. Sun, *Lab Chip*, 2016, **16**, 2254–2264.

88 J. Liu, B. Li, T. Zhu, Y. Zhou, S. Li, S. Guo and T. Li, *Biomicrofluidics*, 2019, **13**, 034114.

89 B. Liu, Z. Ma, J. Yang, G. Gao and H. Liu, *Micromachines*, 2020, **11**, 827.

90 A. Salari, V. Gnyawali, I. Griffiths, R. Karshafian, M. Kolios and S. Tsai, *Soft Matter*, 2017, **13**, 8796–8806.

91 V. Gnyawali, B. U. Moon, J. Kieda, R. Karshafian, M. C. Kolios and S. S. H. Tsai, *Soft Matter*, 2017, **13**, 4011–4016.

92 L. Meng, F. Y. Cai, Q. F. Jin, L. L. Niu, C. X. Jiang, Z. H. Wang, J. R. Wu and H. R. Zheng, *Sens. Actuators, B*, 2011, **160**, 1599–1605.

93 T. H. Wu, L. Y. Gao, Y. Chen, K. Wei and P. Y. Chiou, *Appl. Phys. Lett.*, 2008, **93**, 144102.

94 S. Fujii, K. Kobayashi, K. Kanaizuka, T. Okamoto, S. Toyabe, E. Muneyuki and M. Haga, *Chem. Lett.*, 2010, **39**, 92–93.

95 Y. Yamanishi, R. Tanaka, Y. Arakawa and Y. Nakatsu, Gene transfer by circulating plasma bubble flow, *2017 IEEE 30th International Conference on Micro Electro Mechanical Systems (MEMS)*, 2017, pp. 444–447.

96 C. Wang, J. Cao, Y. Zhou and X. H. Xia, *Talanta*, 2018, **176**, 646–651.

97 B. D. Liu, J. C. Sun, D. S. Li, J. Zhe and K. W. Oh, *Microfluid. Nanofluid.*, 2016, **20**, 155.

98 S. Wang, X. Huang and C. Yang, *Lab Chip*, 2011, **11**, 2081–2087.

99 Z. Z. Chong, S. B. Tor, N. H. Loh, T. N. Wong, A. M. Gañán-Calvo, S. H. Tan and N.-T. Nguyen, *Lab Chip*, 2015, **15**, 996–999.

100 S. Wang, X. Huang and C. Yang, *J. Heat Transfer*, 2012, **134**, 051014.

101 D. Ahmed, X. L. Mao, B. K. Juluri and T. J. Huang, *Microfluid. Nanofluid.*, 2009, **7**, 727–731.

102 M. V. Patel, A. R. Tovar and A. P. Lee, *Lab Chip*, 2012, **12**, 139–145.

103 D. Ahmed, A. Ozcelik, N. Bojanala, N. Nama, A. Upadhyay, Y. Chen, W. Hanna-Rose and T. J. Huang, *Nat. Commun.*, 2016, **7**, 11085.

104 D. Ahmed, X. L. Mao, J. J. Shi, B. K. Juluri and T. J. Huang, *Lab Chip*, 2009, **9**, 2738–2741.

105 Y. Xie, D. Ahmed, M. I. Lapsley, M. Lu, S. Li and T. J. Huang, *J. Lab. Autom.*, 2014, **19**, 137–143.

106 Y. Gao, M. Wu, Y. Lin, W. Zhao and J. Xu, *Microfluid. Nanofluid.*, 2020, **24**, 29.

107 A. Zijlstra, D. F. Rivas, H. J. Gardeniers, M. Versluis and D. Lohse, *Ultrasonics*, 2015, **56**, 512–523.

108 Y. Xu, A. Hashmi, G. Yu, X. Lu, H.-J. Kwon, X. Chen and J. Xu, *Appl. Phys. Lett.*, 2013, **102**, 023702.

109 A. De Vellis, D. Gritsenko, Y. Lin, Z. P. Wu, X. Zhang, Y. Y. Pan, W. Xue and J. Xu, *Sens. Actuators, B*, 2017, **243**, 298–302.

110 Y. Lin, C. Gao, Y. Gao, M. Wu, A. A. Yazdi and J. Xu, *Sens. Actuators, B*, 2019, **287**, 312–319.

111 Y. Lin, Y. Gao, M. Wu, R. Zhou, D. Chung, G. Caraveo and J. Xu, *Lab Chip*, 2019, **19**, 3045–3053.

112 J. Feng, J. Q. Yuan and S. K. Cho, *Lab Chip*, 2015, **15**, 1554–1562.

113 D. Ahmed, M. Lu, A. Nourhani, P. E. Lammert, Z. Stratton, H. S. Muddana, V. H. Crespi and T. J. Huang, *Sci. Rep.*, 2015, **5**, 9744.

114 A. Aghakhani, O. Yasa, P. Wrede and M. Sitti, *Proc. Natl. Acad. Sci. U. S. A.*, 2020, **117**, 3469–3477.

115 L. Ren, N. Nama, J. M. McNeill, F. Soto, Z. Yan, W. Liu, W. Wang, J. Wang and T. E. Mallouk, *Sci. Adv.*, 2019, **5**, eaax3084.

116 J. X. Liu, S. J. Li and D. Mitra, *Int. J. Heat Mass Transfer*, 2015, **91**, 611–618.

117 M. J. Jensen, Bubbles in microchannels, *Master Thesis*, Technical University of Denmark, 2002, p. c960853.

118 D. Park, H. Jeon, M. Kim, X. Nguyen, K. Morten and J. Go, 3D microfluidic perfusion cell culture system with linear concentration gradient and air bubble trapping, *2017 19th International Conference on Solid-State Sensors, Actuators and Microsystems (TRANSDUCERS)*, 2017, pp. 281–284.

119 E. Kang, D. H. Lee, C.-B. Kim, S. J. Yoo and S.-H. Lee, *J. Micromech. Microeng.*, 2010, **20**, 045009.

120 W.-F. Fang and A. P. Lee, *Microfluid. Nanofluid.*, 2015, **18**, 1265–1275.

121 J. O. Kwon, J. S. Yang, S. J. Lee, K. Rhee and S. K. Chung, *J. Micromech. Microeng.*, 2011, **21**, 045009.

122 Y. Chen, Z. Fang, B. Merritt, D. Strack, J. Xu and S. Lee, *Lab Chip*, 2016, **16**, 3024–3032.

123 J. Huo, J. Yong, F. Chen, Q. Yang, Y. Fang and X. Hou, *Adv. Mater. Interfaces*, 2019, **6**, 1900262.

124 K. Du, I. Wathuthanthri, J. Ding and C.-H. Choi, *Appl. Phys. Lett.*, 2018, **113**, 143701.

125 A. Ozcelik, D. Ahmed, Y. L. Xie, N. Nama, Z. G. Qu, A. A. Nawaz and T. J. Huang, *Anal. Chem.*, 2014, **86**, 5083–5088.

126 H.-B. Cheng and Y.-W. Lu, *Microfluid. Nanofluid.*, 2014, **17**, 855–862.

127 J. Xu, R. Vaillant and D. Attinger, *Microfluid. Nanofluid.*, 2010, **9**, 765–772.

128 P. F. Hao, C. Wong, Z. H. Yao and K. Q. Zhu, *Chem. Eng. Technol.*, 2009, **32**, 912–918.

129 C. Lee and C.-H. Choi, *Phys. Rev. Lett.*, 2008, **101**, 064501.

130 Y. C. Jung and B. Bhushan, *J. Phys.: Condens. Matter*, 2009, **22**, 035104.

131 M. A. Samaha, H. Vahedi Tafreshi and M. Gad-el-Hak, *Phys. Fluids*, 2011, **23**, 012001.

132 J. Ou, B. Perot and J. P. Rothstein, *Phys. Fluids*, 2004, **16**, 4635–4643.

133 C. Lee, C.-H. Choi and C.-J. Kim, *Exp. Fluids*, 2016, **57**, 176.